Crustal Velocity Structure in Iranian Kopeh-Dagh, from Analysis of P-Waveform Receiver Functions

Gholamreza Nowrouzi[1], Keith F. Priestley[2], Mohsen Ghafory-Ashtiany[1], Gholam Javan Doloei[1], and Daniel J. Rham[2]

1. International Institute of Earthquake Engineering and Seismology (IIEES), I.R. Iran, email: gnowrouzi@iiees.ac.ir
2. Department of Earth Sciences, University of Cambridge, Cambridge, UK

ABSTRACT: *In this study, the crustal velocity structure and depth of Moho is determined under the eastern part of Iranian Kopeh Dagh, North-East Iran that is named Hezar-Masjed mountains. The teleseismic waveform receiver functions technique is used to determine crustal thicknesses in this study. 41 teleseismic earthquakes from three broad-band seismometers installed in the Iranian Kopeh-Dagh, are used to calculate P-wave receiver functions. Receiver functions for each station are generated from events for a wide range of backazimuths. From analysis of receiver functions at KAR, ZOW and HAM stations, the crustal structure is suggested for the Hezar-Masjed area with a Moho depth of 44-50km. Results indicate three main layers; the upper crust has an S-wave velocity between 2.1-3.2km/s and a 10 to 12km thickness, a middle crust with S-wave velocity between 3.2-3.7km/s and a 22 to 25km thickness and the lower crust with S-wave velocity between 3.7-4.4km/s and a 12 to 15km thickness. An S wave velocity between 4.6-4.7km/s indicates the velocity of the Moho at 47km on average and varies from 44 to 50km. Deeper Moho is found under the southern station.*

Keywords: Kopeh-Dagh; Hezar-Masjed mountains; Crustal structure; Moho discontinuity; Teleseismic receiver functions

1. Introduction

The discontinuity between the earth's crust and the mantle (Moho), is a major change in seismic velocities and chemical properties. Depth and lateral variation of the Moho have strong influence on seismic wave propagation and shaking from damaging earthquakes in certain distance ranges [23].

P-waveform teleseismic receiver function analysis is becoming a common method to estimate the formation of major crustal features and the seismic velocities of the crust and uppermost mantle. This technique is used to determine crustal thickness and depth of the Moho in the study area.

A general study of seismic P-wave and S-wave velocities by using arrival time data of regional earthquakes [8] provided seismic structure information beneath Iran with average *Pn* velocity of 8.0± 0.1*km/s*. Surface wave analysis of a few events [6] suggested a one-layer model crust with 45*km* thickness beneath the eastern part of Alborz mountain range. Asudeh [6] showed that the crust and upper mantle in the eastern part of Iran are characterized by low body wave velocities. The gravity field and crustal structure of Iran, in the study by Dehghani and Makris [10], showed that the crustal thickness varies between 36- 47*km*. The first and only deep seismic sounding in Iran was conduced in 1978 between the Lut Block in the east of the country and the Zagros mountain range in the west. The results of this study identified a 40*km* crustal thickness for the central Iranian Plateau [11]. Numerical modeling of the deformation of the Iranian plateau [22] identified that crustal thickening and shear deformation tend to localize near the southwest of the country. Their results specified a 45*km* crustal

thickness along the Alborz mountain range. Based on receiver function analysis of teleseismic data, Mangino and Priestley [18] provided more information on crustal structure of the southern Caspian and Kopeh Dagh region. Receiver function studies from *MAIO* station on south of Mashhad [13-14] identified seismic discontinuities to a depth of about 52*km*.

The purpose of this paper is to determine the crustal seismic velocity structures of the north-east of Iran based on a receiver function analysis of 41 selected teleseismic earthquakes, beneath three stations during 2004.

2. Methodology

Teleseismic body waveform receiver functions have often been used to infer crustal structure beneath isolated seismic stations [2, 3, 4, 5, 15, 16, 19, 20] and in this experiment are employed to image the lithospheric structure by exposing *Ps* converted seismic phases.

Based on the mentioned studies, computing a receiver function is a deconvolution problem. The simple frequency domain deconvolution e.g. [16] only work in the ideal case, because recorded signals, even broadband signals are band limited, due to random noise that will always be present in seismograms. The most commonly employed method in receiver function studies is a water-level-stabilized, frequency-domain division. In the case of most temporary deployments, we never have enough observations from all azimuths, and signals from smaller events must be incorporated, which lead to difficult deconvolutions and noisy receiver functions. Then the choice of a deconvolution technique may make a difference.

In this study, an iterative time domain deconvolution is commonly used to estimate large-earthquake source time functions [17]. The iterative time-domain approach has several desirable qualities such as a constraint on the spectral shape at long periods that can be advantageous in receiver-function analyses and an intuitive stripping of information from the original signal, garnering the largest, most important features first, and then extracting the details [17].

In receiver-function estimation, the foundation of the iterative deconvolution approach is a least-squares minimization of the difference between the observed horizontal seismogram and a predicted signal generated by the convolution of an iteratively updated spike train with the vertical-component seismogram. For this discussion, it is assumed that we are estimating the radial receiver function. First, the vertical component is cross-correlated with the radial component to estimate the lag of the first and largest spike in the receiver function (the optimal time is that of the largest peak in the absolute sense in the cross-correlation signal). Then the convolution of the current estimate of the receiver function with the vertical-component seismogram is subtracted from the radial-component seismogram, and the procedure is repeated to estimate other spike lags and amplitudes. With each additional spike in the receiver function, the misfit between the vertical and receiver-function convolution and the radial-component seismogram is reduced, and the iteration halts become insignificant when the reduction in misfit with additional spikes.

The first-order information about the crustal structure under a station can be derived from the radial receiver function which is dominated by *P*-to-*S* converted energy from a series of velocity discontinuities in the crust and upper mantle. Because of the large velocity contrast at the crust-mantle boundary, the Moho *P*-to-*S* conversion, *Ps* is often the largest signal following the direct *P*.

In real situations, identifying the Moho *Ps* and the multiples and measuring their arrival times on a single receiver function trace can be very difficult due to background noise, scatterings from crustal heterogeneities, and *P*-to-*S* conversions from other velocity discontinuities. To increase the signal/noise ratio (*SNR*), multiple events are used and their receiver functions are stacked. Such stacking is usually done in the time domain for a cluster of events, e.g. [19].

In this study, the crustal structure resolved is divided by receiver function modeling based on the changes in velocity gradient in the velocity-depth profiles, rather than using the absolute *P*-wave velocity to classify the different parts of the crust. The absolute velocity modeled at any depth is of less importance than the positions and magnitudes of velocity contrasts in the models [9].

The Ammon [3] technique is used which estimates the absolute amplitude of receiver function. Working with true amplitudes illustrates the decrease in the amplitude of the converted phases with increasing source-receiver distance. The true amplitudes are important when estimating the influence of scattering on the receiver function estimates [3].

3. Geology of the Studied Region

The Kopeh-Dagh trends at 120-300 degrees for 700*km* through northeast Iran and Turkmenistan between the Caspian Sea and the border of Afghanistan, see Figure (1). The range is up to 3000*m* in altitude, some 2000*m* higher than the Turkmen foreland to the north. In the Hezar-Masjed Mountains, the Kopeh-Dagh reaches altitudes of more than 3000*m*.

The right-lateral Ashgabat Fault lies at the northern margin of the range [1]. This fault has a component of thrust motion to the north [21]. The Kopeh-Dagh range is separated in the south from the eastern Alborz mountain range by several reverse faults. The west central part drains to the Caspian Sea through the Atrak River system and the southeastern part drains to the Kashaf-Rud depression.

The Kopeh-Dagh mountain system is made up mainly of Cretaceous-Jurassic marine miogeosynclinal sediments. At Ag-Darband, 110*km* east of Mashhad, it contains a core of Triassic-Perecamberian rock units with basic volcanics, tightly folded and sliced in the early Kimmerian-Late Hercynian tectonic phase. This core is transgressed in marked angular unconformity by Jurassic sand stones and shales of the Kopeh-Dagh sedimentary sequence. In late Palaeocene to early Eocene time, the last marine transgression covered the northern and eastern part of Kopeh-Dagh basin. The last epeirogenic movement occurred in late Eocene-early Oligocene time, uplifting the entire region [7]. Therefore, the Kopeh-Dagh formed a mountain belt since early-to-middle Oligocene time.

4. Teleseismic Data and Receiver Functions

Three broadband seismic stations have recorded the teleseismic data used in this study. These stations installed in Iranian Kopeh-Dagh or Hezar-Masjed mountains, operated from May 2004 to December 2004, see Figure (1) and Table (1). As shown in Figure (1), the stations cross the Hezar-Masjed mountains well.

Table 1. Locations of stations, bedrock and number of receiver functions used in this study.

Station Code (Full Name)	Lat. (°*N*)	Long. (°*E*)	Alt. (*m*)	Bedrock of Station	R.F.
KAR (Kardeh)	36.66	59.66	1316	Limestone, Micritic and Marl (Jurassic)	41
ZOW (Zow-e-Sofla)	36.74	59.94	1136	Limestone, Light to Gray, Oolitic (Lower Cretaceous)	13
HAM (Hammam Qaleh)	36.93	59.77	1240	Shail, Dark Gray to Black (Lower Cretaceous)	25

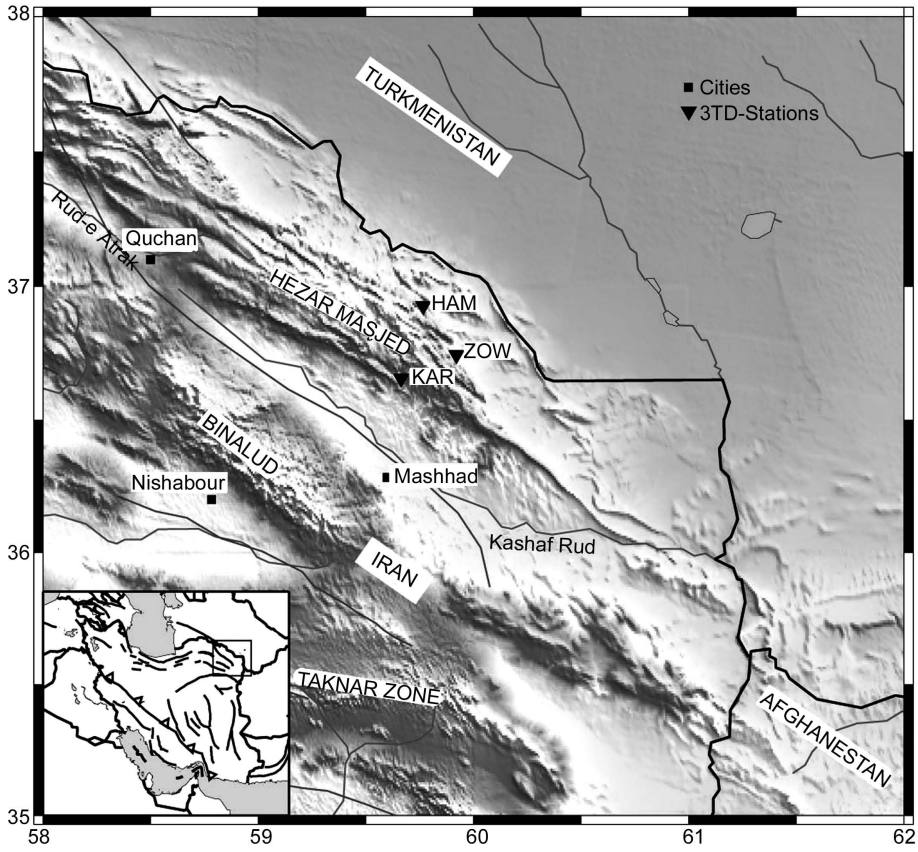

Figure 1. Topographic relief of north-east of Iran. Triangles represent the seismic stations. Quadrangles indicate the cities. Major tectonic provinces are labeled.

The stations were equipped with Guralp *CMG-3TD*, the three-component sensors that had a flat velocity response between 0.02 and 120*s*, sensitivity: 2000*V/m/s*.

During the operation time, more than forty teleseismic earthquakes with acceptable quality were recorded by the stations. The number of receiver functions for stations varies from 13 to 41, depending on the length of recording period, technical problems and background noise level of the station, see Table (1).

The events are selected from the global earthquakes with $Mw \geq 5.6$ and distance range from 30 to 95 degree to the center of the stations.

To process the seismograms, the Seismic Analysis Code (*SAC*) software is used in this study to filter the data with a band pass Butterworth filter to remove the outside of the frequency band of interest, (e.g. 0.001-5.0 *Hz*). Receiver functions were computed using the iterative deconvolution method developed by Herrmann and Ammon [12]. A time window of 100*s* in length, starting 20*s* before the *P* onset is used to cut the *P* waveform from raw velocity records. The two horizontal components are rotated to the radial and tangential directions. The Gaussian filter parameter (α) is chosen to be 1 which corresponds to a cutoff frequency of 0.48*Hz*. These emphasize energy in the long period band.

5. Analysis of Receiver Functions

The number of receiver functions that have been analyzed to derive the main features of the crustal structure beneath each station is presented in Table (2). The incoming back-azimuths of these events and all receiver functions of stations are represented in Figure (2). The conversion phases from the Moho is indicated as *Ps* in Figure (2), the *Pp* phases is direct *P* wave and as a reference time, the *PpPs* phase is a crustal multiple conversion phase.

Data at *KAR* station are better than others and it is easier to find direct conversion. The formations beneath the stations are different as there is more complexity beneath the *ZOW* and *HAM* stations.

The negative amplitude seen at near 8*sec* at *KAR* station, probably represents a *P-S* conversion from an upper-mantle Low Velocity Zone (*LVZ*), but it is questionable. At *KAR* station, till 90 degrees, the Moho is at 4-5*sec* and then for other azimuths at ~6 sec, there are three main effects for this inclination; dipping reflectors, scattering field and anisotropy, that could be interpreted as a south-west dipping interface [13], however an exact anisotropy study is still needed to distinguish the origin of this phase.

After obtaining the receiver functions, the following steps are taken to prepare velocity-depth functions as:

- An initial velocity-depth model is defined based on previous investigations in the area, e.g. [14].
- The radial receiver function is inverted by minimizing the difference between the observed receiver function and the synthetics computed for those models, while simultaneously constraining the model smoothness.
- One of the best-fitting models is selected, and the main features of the structure are derived by grouping the thin layers with similar velocities into a single thicker layer.
- The adjusted model is used as an initial model and inversion is repeated regarding observed radial receiver function.

Based on this study, an example of the structural modeling beneath each station is presented, see Figures (3) to (5). The chosen example for each station is one that its thicknesses are the same as the average thicknesses for that station. The final results are presented in Table (2).

Table 2. The final results of modeling beneath the stations.

Station	Upper Crust h_u (km) , V_s (km/s)	Middle Crust h_m (km) , V_s (km/s)	Lower Crust h_l (km) , V_s (km/s)	Depth of Moho (km)
HAM	10 , 2.8 – 3.5	22 , 3.4 – 3.7	12 , 3.7 – 4.4	44
ZOW	10 , 2.4 – 3.4	25 , 3.0 – 3.9	12 , 3.9 - 4.6	47
KAR	12 , 2.0 - 3.2	23 , 3.5 – 3.6	15 , 3.4 – 4.2	50

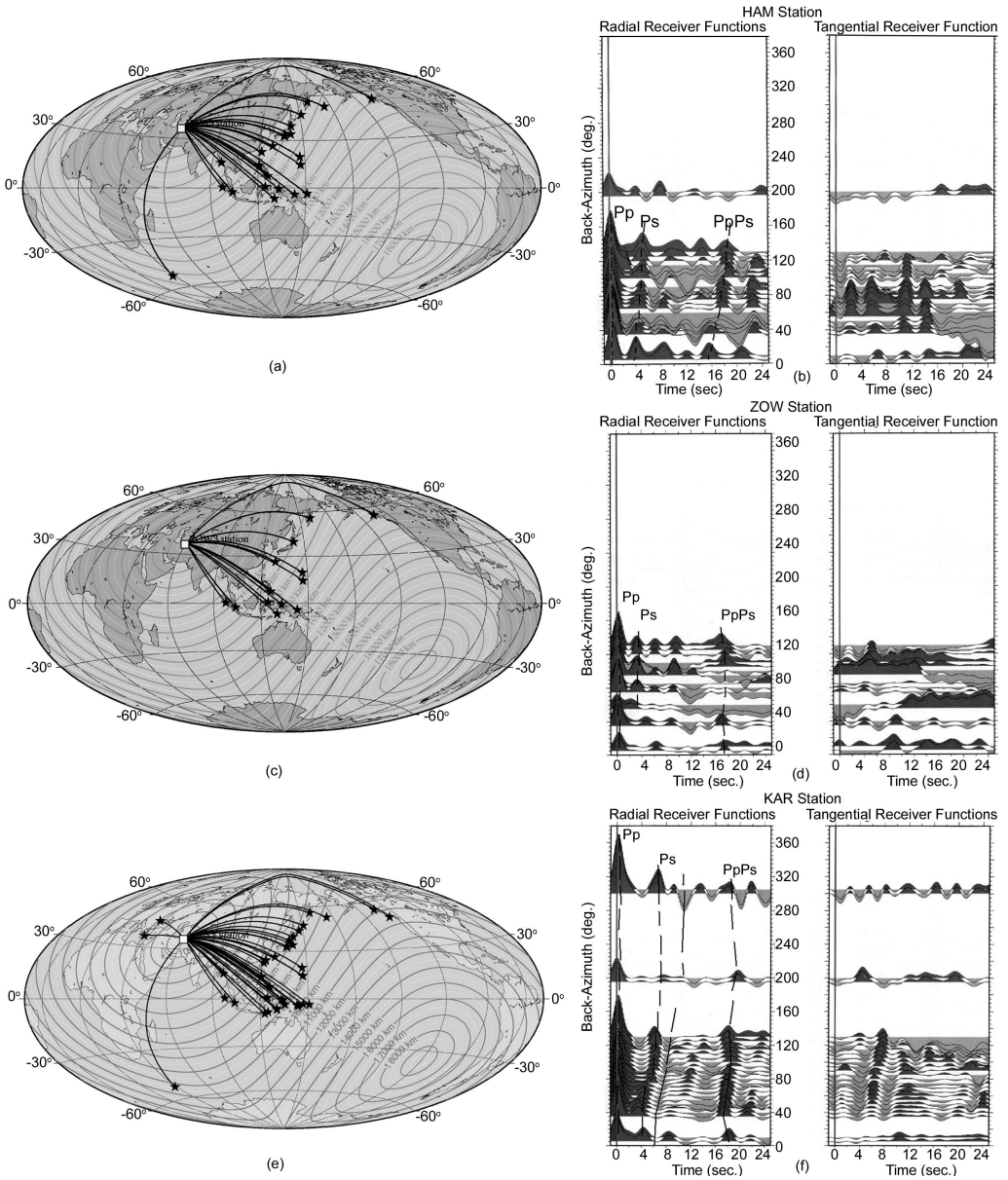

Figure 2. a, c, e) Location of teleseismic events and the distance of them to stations for *HAM*, *ZOW* and *KAR* respectively. b, d, f) Radial (left) and tangential (right) receiver functions as a function of back-azimuth deduced from teleseismic events recorded at *HAM*, *ZOW* and *KAR* stations respectively.

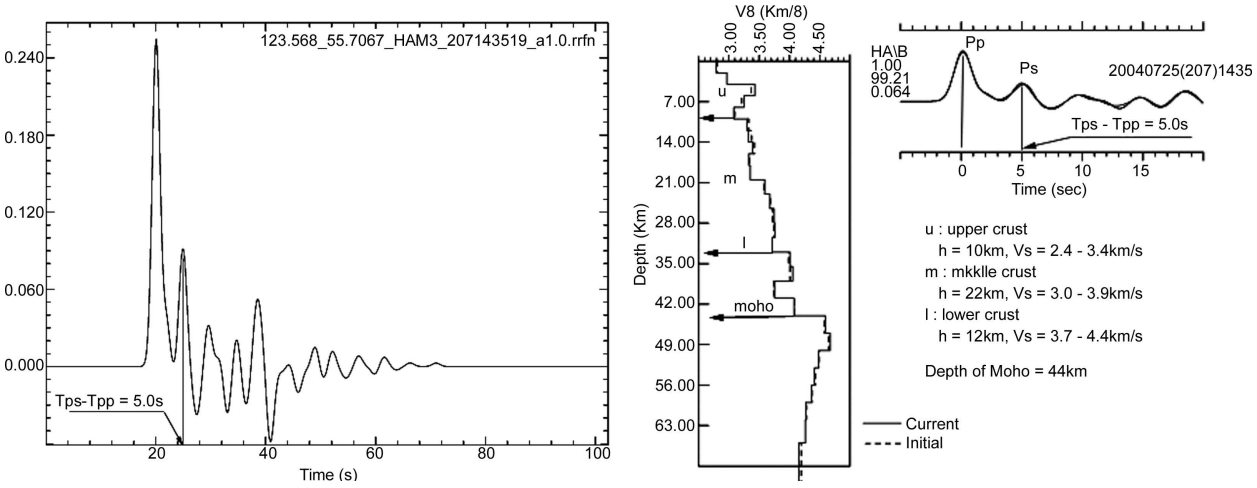

Figure 3. a) Radial receiver functions obtained from 2004207143519 event (Lat: -2.422, Long: 103.96, Depth: 44, Mag: 6.1, Distance: 6562km, *BAZ*: 123 degree) recorded at *HAM* station. b) Fitted model and its interpretation.

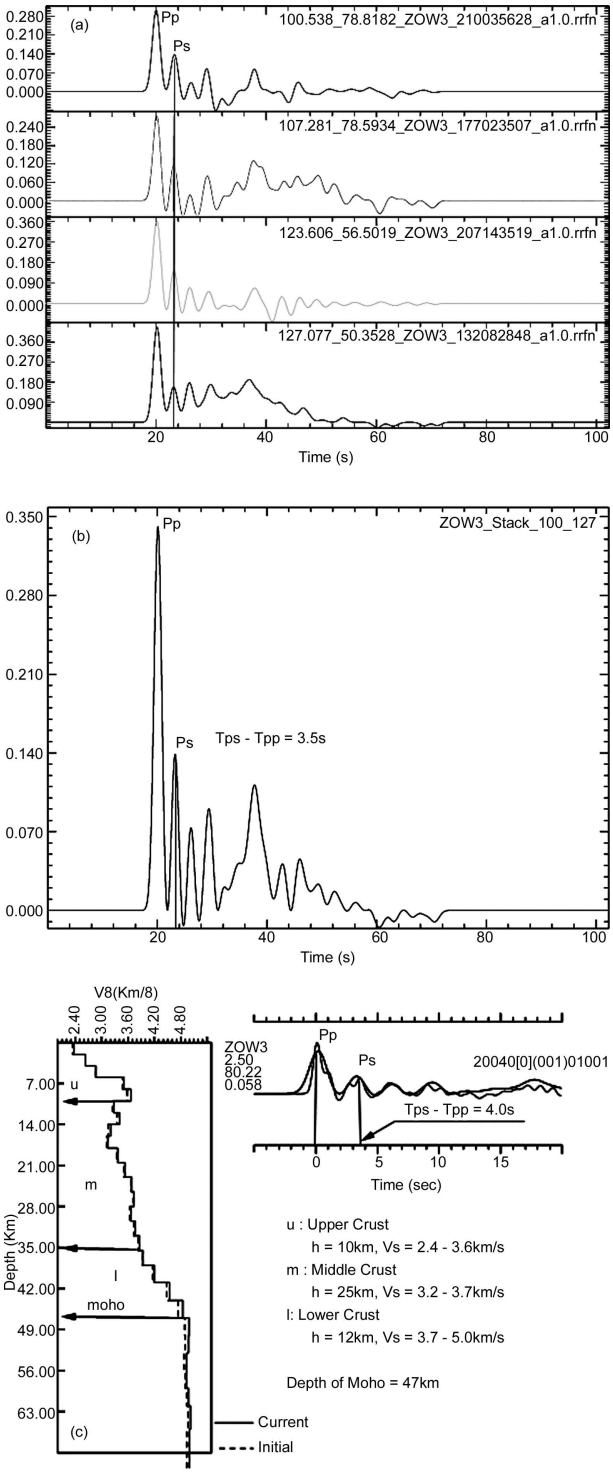

Figure 4. a) Radial receiver functions obtained from four events, recorded at *ZOW* station. b) Stacked of receiver functions presented in (a). c) Fitted model and its interpretation.

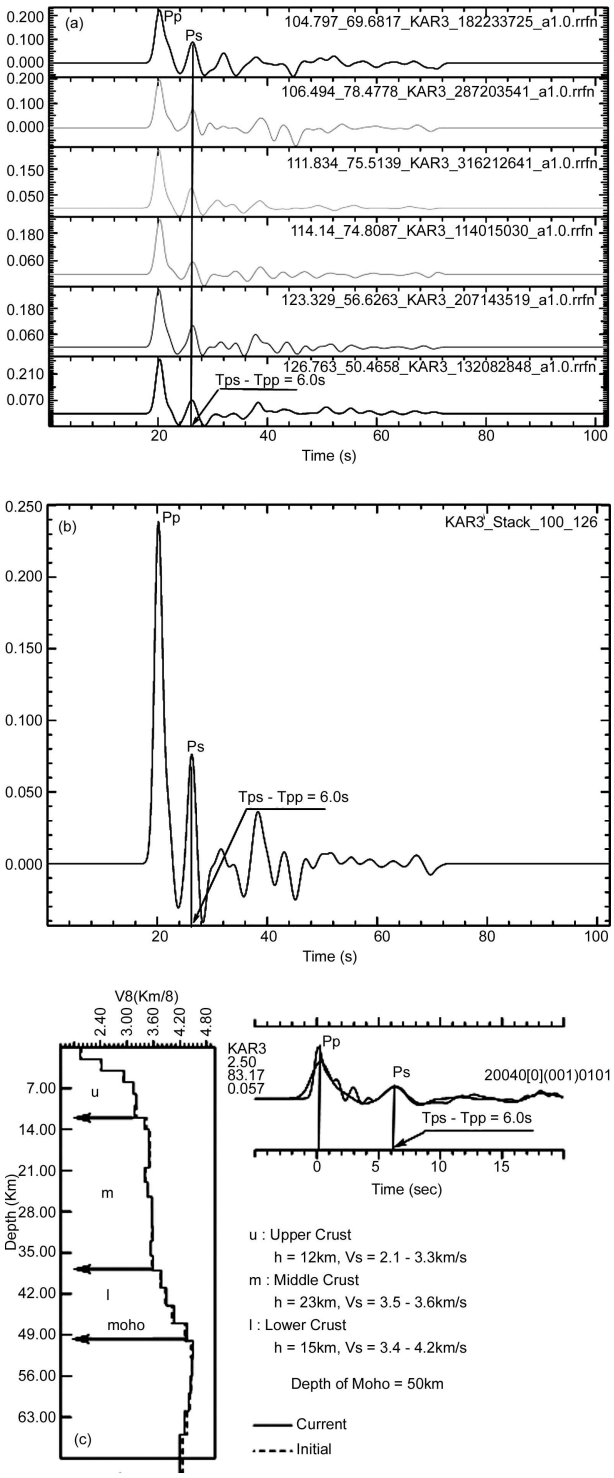

Figure 5. a) Receiver functions obtained from six events, recorded at *KAR* station. b) Stacked of receiver functions presented in (a). c) Fitted model and its interpretation, the intracrustal discontinuity phases are clear between the *Pp* and *Ps* times.

6. Discussion and Conclusions

Teleseismic receiver function modeling constrains a crustal velocity structure across the Iranian Kopeh-Dagh. The crustal thickness varies from 44 to 50 *km*. The upper crust is 10 to 12*km* thick, the middle crust is 22 to 25*km* thick and the lower crust is 12 to 15*km* thick. The *S* wave velocity for these three main layers of crust in the studied area is 2.1-3.2, 3.2-3.7 and 3.7-4.4*km/s* respectively.

This receiver function modeling is one of the first attempts to derive the main features of the crust below the area, therefore the ability to compare these results

to the other studies is limited. The *Pn* velocity of 8.0 ± 0.1*km/s* has been used as a main characteristic of clower crust and Moho boundary based on Chen et al [8]. Our results show the Moho to be ~5*km* deeper than Dehghani and Makris [10] results. The results for *HAM* station that are nearest to *ABKT* are in good agreement with Mangino and Priestly [18] results. Javan Doloei [13] and Javan Doloei and Ashtiany [14] have defined the crustal model beneath *MAIO* station in Mashhad area, using receiver function. They have suggested a 52*km* depth for the Moho. In our study, the depth of the Moho in *KAR* station is in a good agreement with the results for the *MAIO* station.

Acknowledgments

This work was partly supported by the International Institute of Earthquake Engineering and Seismology (*IIEES*), Iran and by the Department of Earth Sciences, University of Cambridge, UK. The authors would like to thank both of these respected research institutes. We gratefully acknowledge the helpful comments and suggestions of the four anonymous reviewers.

References

1. Allen, M., Jackson, J., and Walker, R. (2004). "Late Cenozoic Reorganization of the Arabia-Eurasia Collision and the Comparison of Short-Term and Long-Term Deformation Rates", *Tectonics*, **23**, TC2008, doi:10.1029/2003 TC001530.

2. Ammon, G.J., Randall, G.E., and Zandt, G. (1990). "On the Nonuniqueness of Receiver Functions", *J. Geophys. Res.*, **95**, 15303-15318.

3. Ammon, G.J. (1991). "The Isolation of Receiver Effects from Teleseismic P Waveforms", Bull. Seism. Soc. Am., **81**, 2504-2510.

4. Ammon, C.J. and Zandt, G. (1993). "Receiver Structure Beneath the Southern Mojave Block", *BSSA*, **83**, 737-755.

5. Ammon, C.J. (1997). "An Overview of Receiver-Function Analysis: Pennsylvania State Univ.", http://eqseis.geosc.psu.edu/~ cammon/HTML/ RftnDocs/rftn01.html.

6. Asudeh, I. (1982). "Seismic Structure of Iran from Surface and Body Wave Data", *Geophys. J. R. Asrron. Soc.*, **71**, 715-730.

7. Berberian, M. and Kings, G.C.C. (1981). "Towards a Paleogeography and Tectonic Evolution of Iran", *Canadian, J. Earth Sci.*, **18**, 210-265.

8. Chen, C.Y., Chen, W.P., and Molnar, P. (1980). "The Uppermost Mantle P Wave Velocities Beneath Turkey and Iran", *Geophys. Res. Lett.*, **7**, 77-80.

9. Darbyshire, F.A., Priestley, K.F., White, R.S., Stefansson, R., Gudmundsson, G.B., and Jakobsdottir, S.S. (2000). "Crustal Structure of Central and Northern Iceland from Analysis of Teleseismic Receiver Functions", *Geophys. J. Int.*, **143**, 163-184.

10. Dehghani. G.A. and Makris, J. (1984). "The Gravity Field and Crustal Structure of Iran", *Neues Jahrb, Geol. Palaentol*, **168**, 215-229.

11. Giese, P., Makris, J., Akasheh, B., Roewer, P., Letz, H., and Mostaaanpour, M. (1984). "The Crustal Structure in Southern Iran Derived from Seismic Explosion Data", *Neues Jahrb, Geol. Palaentol.*, **168**, 230-243.

12. Herrmann, R.B. and Ammon, C.J. (2002). "Surface Waves, Receiver Functions and Crustal Structure, Computer Programs in Seismology", Version 3.30.

13. Javan Doloei, Gh. (2003). "Transfer /Receiver Functions and its Application on Crustal Structure of Uppsala, Tehran and Mashhad Area", Ph.D Thesis, International Institute of Earthquake Engineering and Seismology (IIEES).

14. Javan Doloei, Gh. and Ghafory-Ashtiany, M. (2004). "Crustal Structure of Mashhad Area from Time Domain Receiver Functions Analysis of Teleseismic Earthquake", Research Bulletin of Seismology and Earthquake Engineering, (27), 30-38 (in Persian).

15. Langston, C.A. (1977). "Corvallis, Oregon, Crustal and Upper Mantle Receiver Structure from Teleseismic P and S Waves", *BSSA*, **67**, 713-724.

16. Langston, C.A. (1979). "Structure under Mount Rainier, Washington, Inferred from Teleseismic Body Waves", *J. Geophys. Res.*, **84**, 4749-4762.

17. Ligorria, J.P. and Ammon, C.J. (1999). "Iterative

Deconvolution and Receiver-Function Estimation", *BSSA*, **89**(5), 1395-1400.

18. Mangino, S. and Priestley, K. (1998). "The Crustal Structure of the Southern Caspian Region", *Geophys. J. Int.*, **133**, 630-648.

19. Owens, T.J., Zandt, G., and Taylor, S.R. (1984). "Seismic Evidence for Ancient Rift Beneath the Cumberland Plateau, Tenessee: A Detailed Analysis of Broadband Teleseismic P Waveforms", *J. Geophys. Res.*, **89**, 7783-7795.

20. Owens, T.J. and Crosson, R.S. (1988). "Shallow Structure Effects on Broadband Teleseismic P Waveforms", *BSSA*, **78**(1), 96-108.

21. Priestley, K., Baker, C., and Jackson, J. (1994). "Implications of Earthquake Focal Mechanism Data for the Active Tectonics of the South Caspian Basin and Surrounding Regions", *Geophys. J. Int.*, **118**, 111-141.

22. Sobouti, F. and Arkani-Hamed, J. (1996). "Numerical Modeling of the Deformation of the Iranian Plateau", *Geophys. J. Int.*, **126**, 805-818.

23. Zhu, L. and Kanamori, H. (2000). "Moho Depth Variation in Southern California from Teleseismic Receiver Functions", *J. of Geophysical Research*, **105**(B2), 2969-2980.